Nanoscale Horizons

COMMUNICATION

Check for updates

A double helical 4H assembly pattern with secondary hierarchical complexity in an Ag$_{70}$ nanocluster crystal†

Tao Chen,[a] Sha Yang,[b] Qinzhen Li,[a] Yongbo Song,[c] Guang Li, [ID] *[a] Jinsong Chai*[c] and Manzhou Zhu [ID] *[bc]

The hierarchical assemblies of well-defined structural nanoclusters can help to better understand those of biologically important molecules such as DNA and proteins. Herein, we disclose the synthesis and characterization of a new silver nanocluster, that is Ag$_{70}$(SR)$_{42}$(PPh$_3$)$_5$ (Ag$_{70}$-TPP). Directed by the ligands, Ag$_{70}$-TPP nanoclusters undergo self-hierarchical assembly into a highly space-efficient complex secondary structure of a double helical 4H (DH4H) close packing pattern. The chirality of Ag$_{70}$-TPP, and the van der Waals forces interactions between the ligands are believed to drive its DH4H arrangement, and the observed interlocking of the phosphine ligands of adjacent Ag$_{70}$-TPP nanoclusters also contributed. Overall, this work has yielded important and unprecedented insights into the internal structure and crystallographic arrangement of nanoclusters.

New concepts

Nanoclusters with hierarchical assembly characteristics have potential applications in many scientific fields. Most known nanoclusters show simple packing patterns, which largely limits the research progress on the internal assembly of crystal structures. In this work, a new Ag$_{70}$(TBBT)$_{42}$(TPP)$_5$ nanocluster was structurally determined by single crystal X-ray crystallography (SCXC), and a double helical 4H (DH4H) packing mode with complex secondary structure assembly is discovered in its crystal structure. By changing the phosphine ligands on the nanoclusters, the complex DH4H packing mode can be transformed into a simple 2H assembly. Multiple van der Waals forces (C–H···π, π···π, and H···H) between Ag$_{70}$ molecules are considered to be the key factor in maintaining the DH4H packing mode. We believe that our study makes a significant contribution to the understanding of the origin of the arrangement of functional building blocks into ordered hierarchy architectures.

Large and important biomolecules such as DNA, RNA, and proteins are characterized by primary, secondary, and/or more complex structures,[1–3] achieved by self-assembly behavior, self-folding, and/or intermolecular interactions.[4] Of these different assembly modes, hierarchical assembly offers the richest functionality, since secondary structures can result in functional groups that would otherwise be far apart being placed in close proximity, as is the case for enzymes. In this context,

nanomaterials with a biomimetic hierarchical structure can be endowed with biomolecule-like properties. In addition, benefitted by the inherent properties of nanomaterials, this strategy will make it possible to construct biomimetic nanomaterials with more excellent performance than biomolecules.[5,6] Such self-assembly can be driven by the entropic maximization of packing density, electrostatic attraction, and cDNA binding,[7–9] and therefore surface modifications are usually made to discrete NPs to guide their assembly, based on these drivers.[10] For example, gold-based NPs modified with amino acids or peptides can assemble into highly complex and well-defined nanoscale superstructures exhibiting exceptionally strong chiroptical activity.[11,12] These achievements have advanced the field, but progress remains frustrated by the more fundamental problem that nanoparticles exist as polydispersions (no two are the same), and their surface layers and core structure are unclear.

Ultrasmall nanoparticles (nanoclusters, < 2 nm in size) with well-defined crystal structures and unique quantum confinement effects have attracted increasing attention in the

[a] *School of Physics and Materials Science, Institute of Physical Science and Information Technology, Anhui Key Laboratory of Information Materials and Devices, Anhui University, Hefei, Anhui, 230601, People's Republic of China. E-mail: liguang1971@ahu.edu.cn*

[b] *Institutes of Physical Science and Information Technology, Key Laboratory of Structure and Functional Regulation of Hybrid Materials of Ministry of Education, Anhui University, Hefei, Anhui, 230601, China. E-mail: zmz@ahu.edu.cn*

[c] *Department of Chemistry and Centre for Atomic Engineering of Advanced Materials, Anhui Province Key Laboratory of Chemistry for Inorganic/Organic Hybrid Functionalized Materials, Anhui University, Hefei, Anhui, 230601, China. E-mail: chaijs@ahu.edu.cn*

fundamental and applied sciences.[13–15] Entire nanocluster crystal structures can be solved using single-crystal X-ray diffraction, which greatly informs about the forces and factors that determine assembly behavior at the atomic level.[16,17] For example, most nanoclusters adopt either a hexagonal closest packed (HCP) or 2H arrangement with a packing sequence of "ABAB…".[18] However, the face-centered cubic (FCC) arrangement is also known, for example in the crystal of $Au_{30}(SR)_{18}$ reported by the Jin group, and 4H and 6H left-handed helical (6HLH) arrangements have been discovered.[19–21] In addition, $Au_{25}(p\text{-MBA})_{18}^-$ can be used as a building block to organize into well-defined nanoribbons through aurophilic interactions, which significantly enhance the luminescence intensity.[22] However, current research has been mostly limited to first layered hierarchical assembly (helical single strand) with complex structures, and hierarchical assembly modes in second grade (assembly between helical strand, *e.g.* double helix structures in DNA or rhodopsin) are rarely reported in the context of nanoclusters. One exception to this is Zeng's study of atomically precise $[Au_{246}(p\text{-MBT})_{80}]$, which established that nanoclusters can have hierarchical structural complexities at the same level as biomolecules.[23] X-ray diffraction analysis found the thiol ligands on the surface of this nanocluster to self-organize into rotational and parallel patterns *via* a C–H···π interaction. However, this phenomenon was confined to the internal structure of this nanocluster, and the secondary hierarchical assembly of gold or silver nanoclusters in their crystallographic arrangements has rarely been reported.

Herein, we disclose a chiral Ag nanocluster which spontaneously undergoes hierarchical assembly to give a complex secondary structure. This Ag cluster, the formula of which was determined to be $Ag_{70}(TBBT)_{42}(TPP)_5$ (denoted as **Ag_{70}-TPP**, TBBT = 4-*tert*-butylbenzenethiol, and TPP = triphenylphosphine), was synthesized using mixed ligands *via* the "NaSbF$_6$-mediated two-phase ligand exchange method".[24] Based on the irregularity of the surface structure of **Ag_{70}-TPP**, and its chirality, we speculated that the crystallographic arrangement is complex. Further analysis revealed a unique and unprecedented double helical 4H (DH4H) assembly pattern in the unit cells of **Ag_{70}-TPP**, indicating that the cluster assembly forms a complex secondary structure. This unexpected DH4H arrangement of **Ag_{70}-TPP** NCs in the crystal lattice was found to result from the chirality of the **Ag_{70}-TPP** clusters and weak interactions between their ligands. Besides, the crystal structure of **Ag_{70}-TPTP** (TPTP = tri(p-tolyl)phosphine) also pointed out that the ligand is the main influencing factor.

$Ag_{70}(TBBT)_{42}(TPP)_5$ and $Ag_{70}(TBBT)_{42}(TPTP)_5$ NCs were prepared in two steps: (i) the synthesis of water-soluble $Ag_m(SG)_n$ (H-SG = L-glutathione) clusters; (ii) two phase ligand exchange; in which a CH_2Cl_2 solvent containing excess TBBT was mixed with $Ag_m(SG)_n$. Finally, TPP (or TPTP) was added to the above mixed solvent. After overnight reaction, the aqueous solution was removed, and the sample dissolved in CH_2Cl_2 was washed with methanol three times. Black crystals of the nanoclusters were obtained in CH_2Cl_2/CH_3OH at room temperature after 5–7 days.

As shown in Fig. S1 (ESI†), the UV-vis spectrum of **Ag_{70}-TPP** exhibits two distinct absorption peaks at ∼390 and ∼510 nm. According to previous reports, the peak at ∼390 nm (high-energy absorption peak) is mainly attributed to the mixing of metal-to-metal and metal-to-ligand charge-transfer processes (MMCT and MLCT), and the ∼510 nm (low-energy absorption peak) may come from charge transfer within the metal core.[25,26] The **Ag_{70}-TPP** crystals were dissolved in a CH_2Cl_2/CH_3OH mixed solvent for electrospray ionization mass spectrometry (ESI-MS) tests. Two sets of +2 peaks were found in Fig. S2 (ESI†); the main peak at m/z = 7922.2 Da corresponds to the full molecular formula of $[Ag_{70}(TBBT)_{42}(TPP)_5 + K^+ + H^+]^{2+}$ (Cal. 7922.0 Da), and a fragment peak labelled by an asterisk corresponding to the loss of one –PPh$_3$ ligand.[27,28] We undertook an X-ray photoelectron spectroscopy (XPS) study of **Ag_{70}-TPP**, and the results are shown in Fig. S3a (ESI†). In addition, the binding energies of the Ag 3d peaks in **Ag_{70}-TPP** and Ag(0), Ag(I) species were also compared. The binding energy of Ag $3d_{5/2}$ in **Ag_{70}-TPP** is 368.6 eV (Fig. S3b and c), which is higher than that of Ag(0) (367.9 eV), and closer to the binding energy of a Ag(I)-complex (368.7 eV), indicating that the valence of **Ag_{70}-TPP** is between 0 and +1. ^{1}H, ^{31}P, and ^{2}H-NMR spectroscopy were also used to probe the chemical composition and the ligand environments of **Ag_{70}-TPP** (Fig. S4–S6, ESI†), and a detailed description is shown in the ESI.†

Single crystal X-ray crystallography (SCXC) analysis showed that **Ag_{70}-TPP** crystallized in an orthorhombic *Pbca* space group and is a *pseudo*-five-fold symmetric pentagram-like nanocluster (Fig. 1a). The anatomical diagram of the total structure (Fig. 1b) shows that **Ag_{70}-TPP** has a five-fold symmetric Ag_{23} kernel with 10 (111) faces, which can be described as five conjoined tetrahedral domains of FCC Ag_{10} (*i.e.*, 4 (111) faces), indicating that the Ag_{23} kernel in **Ag_{70}-TPP** is a complete decahedral. This kind of decahedral silver core can also be found in large-sized clusters with more than 100 atoms.[29,30] Atomically precise nanoclusters with a decahedral core are summarized in Table S1 (ESI†). Previous reports indicate that nanoclusters with a general size of 20 to 100 metal atoms tend to have icosahedral, FCC, body-centered cubic (BCC) or HCP cores; few nanoclusters of this size have decahedral cores, although some contain incomplete decahedral structures, and it is expected that as the size (number of metal atoms) increases, the partial decahedral structure may evolve to a complete decahedral structure, as is found in **Ag_{70}-TPP**. Furthermore, the Ag–Ag bond lengths of the Ag_{23} kernel range from 2.740 to 3.194 Å (2.904 Å on average).

The top and bottom of the Ag_{23} kernel are capped by two large pentagram-like shells ($Ag_{14}S_{11}$, $Ag_{13}S_{11}$) (Fig. 1c). As shown in Fig. S7 (ESI†), one Ag atom disordered in two positions, occupies 0.85 and 0.15, respectively. Additionally, a $Ag_{20}S_{20}P_5$ circular motif (consists of five Ag_4S_4P units) terminated by phosphine was found to encircle the decahedron Ag_{23} core in the outermost shell (Fig. 1d). All the phosphine ligands form AgS_3P tetrahedrons (Fig. S8, ESI†) with Ag–P bonds ranging from 2.416 to 2.447 Å (2.429 Å on average, Fig. S9, ESI†). The surface of the flat spherical **Ag_{70}-TPP** cluster is
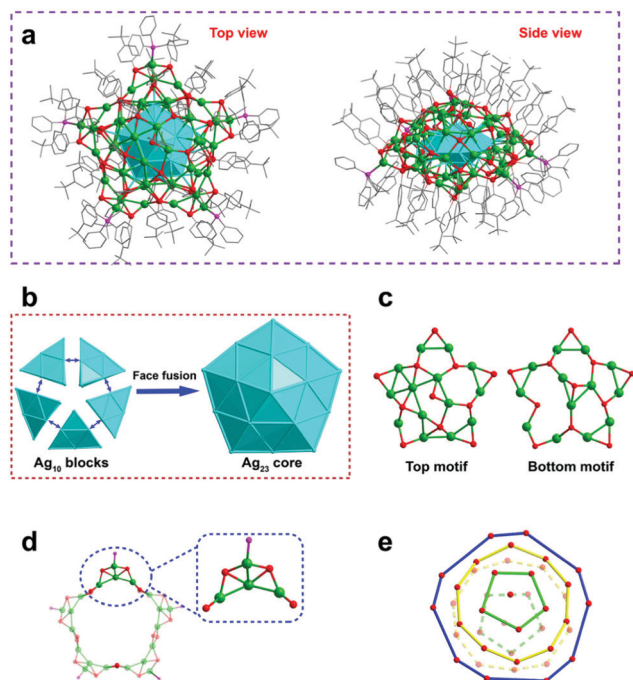
Fig. 1 Structural anatomies of the **Ag$_{70}$-TPP** nanocluster. (a) Top and side views of overall structure; (b) the decahedral Ag$_{23}$ core; (c) Ag$_{14}$S$_{11}$, and Ag$_{13}$S$_{11}$ motifs from the side view; (d) the outmost circular Ag$_{20}$S$_{20}$P$_5$ motif; (e) layer-by-layer distribution of S atoms. Color labels: Ag, turquoise/green; S, red; P, magenta; C, gray. For clarity, all H atoms are omitted.

covered by 42 peripheral thiolate ligands, which can be divided into three categories (Fig. S10, ESI†). The Ag–S bond lengths in **Ag$_{70}$-TPP** range from 2.403 Å to 2.812 Å (average: 2.588 Å). On the other hand, these ligands exhibit a layer-by-layer assembly pattern arranged from pole to equator to opposite pole of the **Ag$_{70}$-TPP**, containing 1, 5, 10, 10, 5, and 1 thiolate ligands for each layer (Fig. 1e).

The overall structure of **Ag$_{70}$-TPP** exhibits C_1 symmetry, indicating its chirality. The Ag$_{23}$ core of Ag$_{70}$ is achiral, which shows a D_{5h} symmetry. Two chiral Ag$_{14}$S$_{11}$ and Ag$_{13}$S$_{11}$ networks were found to cap on the two poles of the decahedral Ag$_{23}$ kernel. Finally, a twisted pentagonal Ag$_{20}$S$_{20}$P$_5$ motif coats on the equator of the Ag$_{23}$ kernel, forming the total chiral framework of the Ag$_{70}$ clusters (Fig. S11, ESI†).[31]

The **Ag$_{70}$-TPP** unit cell contains four pairs of enantiomers (Fig. S12, ESI†). The arrangements of the **Ag$_{70}$-TPP** superlattices are shown in Fig. 2(a–c). As shown in Fig. 2a, enantiomers are arranged along the y axis and z axis, organized into a rectangle superlattice in the (100) plane. In the (001) and (010) planes (Fig. 2b and c), **Ag$_{70}$-TPP** molecules with the same chiral configuration are neatly assembled according the polyline mode (R-configuration **Ag$_{70}$-TPP** NCs are shown in purple, and the S-configuration NCs are shown in golden). The molecules in the β layer can be regarded as the directional arrangement of the α layer through a flip operation, making the crystal a layer-by-layer manner (Fig. 2c). As shown in Fig. 2d, eight **Ag$_{70}$-TPP** molecules in one unit cell can be divided into upper and lower layers. Interestingly, conventional NCs are typically
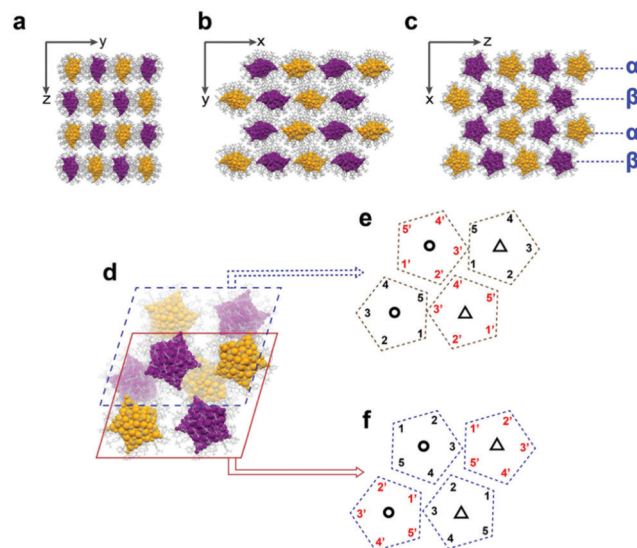

Fig. 2 The self-assembly of **Ag$_{70}$-TPP** clusters on different planes (a) (100), (b) (001), and (c) (010) planes; (d) eight **Ag$_{70}$-TPP** clusters in the same unit cell; (e and f) model diagram of four clusters in the upper and lower layers. (The **Ag$_{70}$-TPP** clusters in two chiral configurations are indicated with different colours. **Ag$_{70}$-TPP** were indicated as pentagons, five phosphine ligands located at the five vertices were numbered and the two poles of the clusters are indicated as Δ and ○.)

packed into superlattices with simple translational or rotational symmetry,[32] while the eight **Ag$_{70}$-TPP** molecules in one unit cell are arranged differently (Fig. 2e and f) and occupy a more complex orthorhombic lattice via monomer rotational, flip, mirror symmetry, and translational operation (Fig. S13, ESI†), such that the eight constituent nanoclusters within an individual unit are symmetrically different and closely packed. This complex arrangement increases the packing efficiency, and the molecules are arranged as closely as possible in the crystal lattice.

Fig. 3 shows the combined observations on the upper and lower layers of the (010) plane. The eight **Ag$_{70}$-TPP** structures within the same unit cell are depicted in eight colours. In the crystal lattice, a complete helix contains four **Ag$_{70}$-TPP** molecules, which arrange around the helical axis along the [100] and
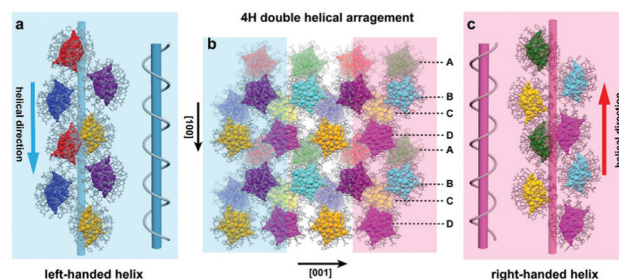

Fig. 3 (a) **Ag$_{70}$-TPP** nanocluster helical arrangement along the [100] direction, (b) double helical 4H arrangement of the **Ag$_{70}$-TPP** nanocluster in the (010) plane, and (c) **Ag$_{70}$-TPP** nanocluster helical arrangement along the [$\bar{1}$00] direction. (Note: the eight clusters of the same unit cell are labeled in different colors).

[1̄00] directions, respectively (Fig. 3a and c). Along the [100] direction, the stacking sequence is "A B C D", which is characteristic of 4H (four layered hexagonal) close packing (Fig. 3b).[33] However, in contrast to traditional 4H the four pairs of **Ag$_{70}$-TPP** are arranged into two helical arrangements (Fig. S14, ESI†), wherein the blue shadow is left-handed and the other in pink shadow is a right-handed helix alternately arranged in adjacent locations (Fig. S14, ESI†), termed as a double helical 4H (DH4H) arrangement, and the average pitch is 26.1 Å. This type of DH4H assembly mode is reminiscent of the helix structure characteristics of biological DNA, but different. The DNA helix biopolymer of nucleic acids is held together by nucleotides which base pair together, with a unique axis, while **Ag$_{70}$-TPP** possesses two parallel helix axes with opposite directions, and connected by weak interactions. (Fig. S15, ESI†). The comparison of the related parameters of the helix of **Ag$_{70}$-TPP** with other helical biological molecules (Alpha-keratin, TMV) is shown in Table S2 (ESI†). Its discovery proves that the self-assembly of nanoclusters such as **Ag$_{70}$-TPP** can be as intricate as is observed for biological molecules.

The secondary structures of proteins are mainly maintained by hydrogen bonds. To explore the factors governing the DH4H-type assembly in **Ag$_{70}$-TPP** nanoclusters, we sought to understand the extent and nature of the interactions between clusters.[34,35] On the surface of the nanocluster, C–H···π and π···π interactions between ligands (Fig. 4a) were found. These interactions can be roughly divided into two types: (i) the interaction between the H atoms of the phosphine and the phenyl ring of the nearby thiolate ligands (Fig. 4b); and (ii) the interaction between multiple thiolate ligands (C–H···π and π···π interactions (Fig. 4c)). The C–H···π distances range from 2.6 Å to 3.2 Å; these are weak interactions, widely distributed in the entire crystal structure, which presumably contribute to its stability.[36,37]

As shown in Fig. 4d and Fig. S16 (ESI†), adjacent NCs are narrowly spaced and C–H···π and H···H interactions are evident, resulting in an intercluster permutation pattern

(Fig. 4d). The shortest distance between neighbouring clusters is only 2.440 Å, suggesting their intermolecular interaction to be strong. The phenyl rings of adjacent phosphines interlock (Fig. 4e and f).[38] The interaction between phosphines is likely to influence the distortion of the cluster. From Fig. S17 (ESI†), the phosphine ligand at the border of the cluster has a large angle of distortion, which is similar to the same poles of a magnet repelling. These intra- and inter-molecular interactions greatly influence the arrangement of clusters in this crystal lattice.
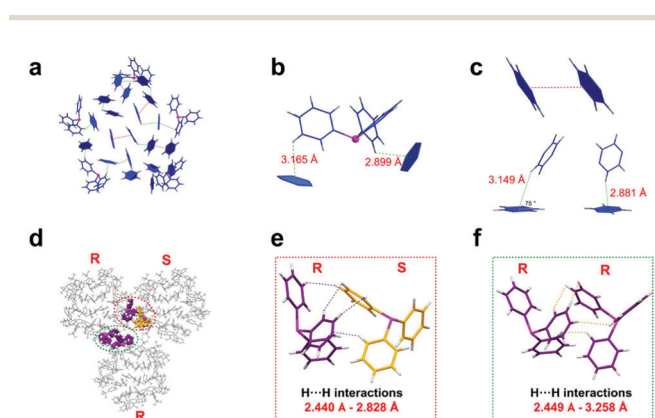
In order to verify whether the phosphine ligand plays an important role in maintaining the DH4H assembly mode.[39,40] Tri(*p*-tolyl)phosphine (TPTP) was selected to replace the TPP ligand during the synthesis of the clusters. The UV-vis spectrum (Fig. S18, ESI†) and TGA (Fig. S19, ESI†) confirmed that the cluster is still **Ag$_{70}$** (denoted as **Ag$_{70}$-TPTP**). In addition, the crystal structure of **Ag$_{70}$-TPTP** was determined by SCXC. As shown in Fig. S20 (ESI†), not only the crystal system (an orthorhombic *Pbca* to a triclinic *P*1̄ space group), but also the assembly pattern (complex DH4H to simple 2H) of **Ag$_{70}$-TPTP** had changed when compared with the **Ag$_{70}$-TPP**. The stacking sequence of **Ag$_{70}$-TPTP** is "A·B·A·B", and **Ag$_{70}$-TPTP** clusters in A-layer and B-layer show opposite chirality (Fig. S20(d–f)). In one unit cell, we found that two groups of phosphine ligands in **R**-, and **S-Ag$_{70}$-TPTP** interlocked each other (Fig. S21a, ESI†) through the C–H···π and H···H interactions. While in the adjacent unit cells, only one pair of phosphine ligand interactions was found (Fig. S21b, ESI†), which is different from that of the **Ag$_{70}$-TPP**.

Conclusions

In summary, the *pseudo*-five-fold symmetric pentagram-like silver nanocluster Ag$_{70}$(TBBT)$_{42}$(TPP)$_5$ was synthesized, and its composition was determined by SCXC, ESI-MS, and NMR analysis. Analysis of the crystal structure of **Ag$_{70}$-TPP** determined its structure to incorporate a complete decahedral Ag$_{23}$ kernel. Due to the coordination preferences and electronic or steric hindrance effects of the mixed ligands (*i.e.* thiolate and phosphine ligands), the intramolecular and intermolecular C–H···π, π···π, and H···H interactions can account for the complex arrangement of **Ag$_{70}$-TPP** in the unit cells. Furthermore, the steric hindrance of the phosphine ligand can be changed to control the way of assembly between molecules to achieve the transformation from complex to simple packing. Collectively, these results show that the secondary structures of sub-nanometer-sized noble metal nanoclusters can be as complex as those found in biological systems, and that structures assembled from nanoclusters can reach not only atomic accuracy but also the same hierarchical assembly as bio-molecules levels.

Fig. 4 (a) The interactions of **Ag$_{70}$-TPP** surface ligands; (b) the intra-molecular C–H···π interaction; (c) the C–H···π interaction and π···π stacking; (d) interaction of adjacent clusters in the lattice; (e) H···H interactions of the cluster with opposite chirality; (f) H···H interactions of the cluster with the same chirality.

Conflicts of interest

The authors declare no competing financial interests.

Acknowledgements

References

1 M. J. Adams, E. N. Baker, T. L. Blundell, E. J. Dodson, G. G. Dodson, M. Vijayan, M. M. Harding, D. C. Hodgkin, B. Rimmer and S. Sheat, *Nature*, 1969, **224**, 491–495.

2 J. D. Watson and F. H. C. Crick, *Nature*, 1953, **171**, 737–738.

3 J. C. Kendrew, *Science*, 1963, **139**, 1259–1266.

4 W. W. Grabow and L. Jaeger, *Acc. Chem. Res.*, 2014, **47**, 1871–1880.

5 Y. Zhao, S. Zhuang, L. Liao, C. Wang, N. Xia, Z. Gan, W. Gu, J. Li, H. Deng and Z. Wu, *J. Am. Chem. Soc.*, 2020, **142**, 973–977.

6 J. Teyssier, S. V. Saenko, D. V. D. Marel and M. C. Milinkovitch, *Nat. Commun.*, 2015, **6**, 6368.

7 P. F. Damasceno, M. Engel and S. C. Glotzer, *Science*, 2012, **337**, 453–457.

8 R. Huang, Y. Wei, X. Dong, X. Wu, C. Du, S. Zang and T. C. W. Mak, *Nat. Chem.*, 2017, **9**, 689–697.

9 S. Y. Park, A. K. R. Lytton-Jean, B. Lee, S. Weigand, G. C. Schatz and C. A. Mirkin, *Nature*, 2008, **451**, 553–556.

10 R. Nidetz and J. Kim, *Nanotechnology*, 2012, **23**, 045602.

11 A. D. Merg, J. C. Boatz, A. Mandal, G. Zhao, S. Mokashi-Punekar, C. Liu, X. Wang, P. Zhang, P. C. A. van der Wel and N. L. Rosi, *J. Am. Chem. Soc.*, 2016, **138**, 13655–13663.

12 H. Fakhouri, M. Perić, F. Bertorelle, P. Dugourd, X. Dagany, I. Russier-Antoine, P. Brevet, V. Bonačić-Koutecký and R. Antoine, *Phys. Chem. Chem. Phys.*, 2019, **21**, 12091–12099.

13 R. Jin, C. Zeng, M. Zhou and Y. Chen, *Chem. Rev.*, 2016, **116**, 10346–10413.

14 I. Chakraborty and T. Pradeep, *Chem. Rev.*, 2017, **117**, 8208–8271.

15 R. S. Dhayal, J. Liao, Y. Liu, M. Chiang, S. Kahlal, J. Saillard and C. W. Liu, *Angew. Chem., Int. Ed.*, 2015, **54**, 3702–3706.

16 P. D. Jadzinsky, G. Calero, C. J. Ackerson and D. A. Bushnell, *Science*, 2007, **318**, 430–433.

17 C. P. Joshi, M. S. Bootharaju, M. J. Alhilaly and O. M. Bakr, *J. Am. Chem. Soc.*, 2015, **137**, 11578–11581.

18 Y. Yang, T. Jia, Y. Han, Z. Nan, S. Yuan, F. Yang and D. Sun, *Angew. Chem., Int. Ed.*, 2019, **58**, 12280–12285.

19 T. Higaki, C. Liu, C. Zeng, R. Jin, Y. Chen, N. L. Rosi and R. Jin, *Angew. Chem., Int. Ed.*, 2016, **55**, 6694–6697.

20 L. Liao, J. Chen, C. Wang, S. Zhuang, N. Yan, C. Yao, N. Xia, L. Li, X. Bao and Z. Wu, *Chem. Commun.*, 2016, **52**, 12036–12039.

21 Z. Gan, J. Chen, J. Wang, C. Wang, M. Li, C. Yao, S. Zhuang, A. Xu, L. Li and Z. Wu, *Nat. Commun.*, 2017, **8**, 14739.

22 Z. Wu, Y. Du, J. Liu, Q. Yao, T. Chen, Y. Cao, H. Zhang and J. Xie, *Angew. Chem., Int. Ed.*, 2019, **58**, 8139–8144.

23 C. Zeng, Y. Chen, K. Kirschbaum, K. J. Lambright and R. Jin, *Science*, 2016, **354**, 1580–1584.

24 T. Chen, S. Yang, Y. Song, J. Chai, Q. Li, X. Ma, G. Li, H. Yu and M. Zhu, *Chem. Commun.*, 2020, **56**, 7605–7608.

25 F. Hu, J. Li, Z. Guan, S. Yuan and Q. Wang, *Angew. Chem., Int. Ed.*, 2020, **59**, 5312–5315.

26 J. Li, Z. Guan, Z. Lei, F. Hu and Q. Wang, *Angew. Chem., Int. Ed.*, 2019, **58**, 1083–1087.

27 L. G. AbdulHalim, M. S. Bootharaju, Q. Tang, S. D. Gobbo, R. G. AbdulHalim, M. Eddaoudi, D. Jiang and O. M. Bakr, *J. Am. Chem. Soc.*, 2015, **137**, 11970–11975.

28 I. Russier-Antoine, F. Bertorelle, R. Hamouda, D. Rayane, P. Dugourd, Ž. Sanader, V. Bonačić-Koutecký, P. Brevet and R. Antoine, *Nanoscale*, 2016, **8**, 2892–2898.

29 T. K. Sau and A. L. Rogach, *Adv. Mater.*, 2010, **22**, 1781–1804.

30 H. Yang, Y. Wang, X. Chen, X. Zhao, L. Gu, H. Huang, J. Yan, C. Xu, G. Li, J. Wu, A. J. Edwards, B. Dittrich, Z. Tang, D. Wang, L. Lehtovaara, H. Häkkinen and N. Zheng, *Nat. Commun.*, 2016, **7**, 12809.

31 H. Han, Y. Yao, A. Bhargava, Z. Wei, Z. Tang, J. Suntivitch, O. Voznyy and R. D. Robinson, *J. Am. Chem. Soc.*, 2020, **142**, 14495–14503.

32 A. Desireddy, B. E. Conn, J. Guo, B. Yoon, R. N. Barnett, B. M. Monahan, K. Kirschbaum, W. P. Griffith, R. L. Whetten, U. Landman and T. P. Bigioni, *Nature*, 2013, **501**, 399–402.

33 M. I. Novgorodova, A. I. Gorshkov and A. V. Mokhov, *Zap. Vses. Mineral. O-va.*, 1979, **108**, 552–563.

34 Y. Li and R. Jin, *J. Am. Chem. Soc.*, 2020, **142**, 13627–13644.

35 T. Chen, S. Yang, J. Chai, Y. Song, J. Fan, B. Rao, H. Sheng, H. Yu and M. Zhu, *Sci. Adv.*, 2017, **3**, e1700956.

36 X. Liu, G. Saranya, X. Huang, X. Cheng, R. Wang, M. Chen, C. Zhang, T. Li and Y. Zhu, *Angew. Chem., Int. Ed.*, 2020, **59**, 13941–13946.

37 A. Nag, P. Chakraborty, M. Bodiuzzaman, T. Ahuja, S. Antharjanam and T. Pradeep, *Nanoscale*, 2018, **10**, 9851–9855.

38 J. Yan, S. Malola, C. Hu, J. Peng, B. Dittrich, B. K. Teo, H. Häkkinen, L. Zheng and N. Zheng, *Nat. Commun.*, 2018, **9**, 3357.

39 Q. Li, J. C. Russell, T. Luo, X. Roy, N. L. Rosi, Y. Zhu and R. Jin, *Nat. Commun.*, 2018, **9**, 3871.

40 L. He, Z. Gan, N. Xia, L. Liao and Z. Wu, *Angew. Chem., Int. Ed.*, 2019, **58**, 9897–9901.